Improved performance of TiO$_2$ in the selective photo-catalytic oxidation of cyclohexane by increasing the rate of desorption through surface silylation

Ana Rita Almeida [a], Joana T. Carneiro [a], Jacob A. Moulijn [a], Guido Mul [b,*]

[a] Catalysis Engineering, Delft University of Technology, Julianalaan 136, 2628 BL Delft, The Netherlands
[b] PhotoCatalytic Synthesis Group, IMPACT Institute, Faculty of Science and Technology, University of Twente, 7500 AE Enschede, The Netherlands

A B S T R A C T

The effect of silylation on the performance of an anatase TiO$_2$ catalyst in the selective photo-oxidation of cyclohexane was investigated using attenuated total reflection Fourier transform infrared (ATR-FTIR) spectroscopy and an illuminated slurry reactor. The rate of cyclohexanone formation showed a dependency on the availability of surface active OH sites and on the desorption rate of cyclohexanone. Two classes of catalysts could be identified: (1) containing less than 1.0 wt.% Si where the cyclohexanone formation rate is decreased by silylation due to a decrease in OH availability and (2) containing more than 1.0 wt.% Si where the improved desorption rate becomes dominant over the decreasing OH availability, and the cyclohexanone formation rate observed in an illuminated slurry reactor is increased. ATR-FTIR results confirmed the linear increase in the rate of cyclohexanone desorption as a function of increasing Silane content of the TiO$_2$ surface. Because of this enhanced desorption, silylation also resulted in a decrease in rate of formation of surface deactivating carbonate and carboxylate species on TiO$_2$.

© 2010 Published by Elsevier Inc.

1. Introduction

Photo-catalysis is widely applied in the decomposition of contaminants from water and air [1]. Among various semi-conductor materials, TiO$_2$ is the most investigated catalyst and used in commercial water purification [2]. The use of TiO$_2$ to selectively synthesize organic compounds at mild conditions is also of interest [3]. However, low conversions and strong deactivation of TiO$_2$ catalysts prevent these photo-catalytic processes from being commercially applied [4–8]. The reason for TiO$_2$ deactivation is the formation of surface-bound carbonates and carboxylates, as observed in ATR-FTIR studies. The formation of these species in the selective cyclohexane oxidation was proposed to be the result of slow desorption of cyclohexanone, which leads to over-oxidation [8]. Transient studies confirmed that cyclohexanone desorption is slow, and requires in the dark almost 30 min to desorb from a pre-illuminated TiO$_2$ catalyst into cyclohexane [9]. In order to decrease the rate of deactivation in cyclohexane oxidation, desorption of cyclohexanone should be stimulated. Several strategies can be followed to achieve this, such as the use of solvents [10–12], the use of elevated temperatures [13] or catalyst modification. In this research, the last option has been evaluated, in particular the modification of the TiO$_2$ surface by silylation. This method is

commonly applied for Ti-substituted mesoporous silica catalysts to reduce desorption limitations of polar products in oxidation reactions [14–16]. In these cases, silanol groups from the mesoporous support are exchanged with methylated silane groups, like trimethylsilanes. But also silylation of commercial TiO$_2$ has been applied, and in general, a decrease in surface hydrophilicity and affinity to polar molecules has been observed [17,18]. It will be demonstrated in the present paper by data obtained from in situ ATR-FTIR studies that the hydrophilicity of a commercial TiO$_2$ catalyst is indeed decreased by coupling trimethylsilane groups to its surface, stimulating desorption of cyclohexanone formed by photo-catalytic cyclohexane oxidation and thus reducing the rate of catalyst deactivation.

2. Experimental

2.1. Catalyst synthesis

The photo-catalyst used in this study was Hombikat UV100 TiO$_2$ (Sachtleben) of 100% anatase crystallinity (determined by XRD), a S_{BET} of 337 m^2/g and a primary particle size of approximately 5 nm [7]. Hexamethyldisilazane (HMDS) from Fluka was chosen as the silylating agent, because of its high reactivity [19,20]. The silylation method applied is similar to the one described by Fadeev et al. [21]. The catalyst was dried overnight at 120 °C, and 0.5 g of TiO$_2$ was mixed with different volumes of HMDS in 10 mL of

toluene (99.5% from Sigma Aldrich), in a magnetically stirred round bottom flask with a reflux cooler. The synthesis was carried out at room temperature for 24 h, after which the silylated TiO_2 materials were filtered, washed with toluene and dried overnight at 120 °C. Four silylation batches were made with 0.02, 0.06, 0.08 and 0.15 g of HMDS.

2.2. Catalyst characterization

X-ray fluorescence (XRF) measurements were done on a Panalytical PW 1480 spectrometer, and the silicon content (wt.%) in the silylated TiO_2 catalysts was calculated with the so-called Superq routine. The silylated TiO_2 catalysts were characterized by diffuse reflectance infrared spectroscopy (DRIFTS) on a Bruker IFS 66 spectrometer. The catalyst powders were introduced into a DRIFTS cell (Spectratech) and dried for 30 min at 120 °C. All absorbance and single-beam spectra were collected with 128 averaged scans and $4 cm^{-1}$ spectral resolution against a KBr background. Thermogravimetric analysis (TGA) was performed on a Mettler Toledo TGA/SDTA851e. The samples were heated from 25 to 600 °C at a heating rate of 10 K/min under 10 mL/min He flow. Solid-state ^{29}Si magic angle spinning nuclear magnetic resonance (^{29}Si MAS NMR) was performed on a Bruker Avance 400 spectrometer, using a 5-mm zirconium rotor, with spinning speed of 11 kHz. The spectral window was 25,063 Hz, with 50 ms acquisition time and 15 s acquisition delay.

2.3. Cyclohexane photo-catalytic oxidation – ATR-FTIR

The catalysts were dried at 120 °C for 1 h in static air and suspended in toluene at a concentration of 3.67 g/L. The suspensions were treated for 30 min in a 35-kHz Elmasonic ultrasonic bath; 2 mL of this suspension was spread on a ZnSe crystal and dried in vacuum overnight.

The in situ ATR-FTIR setup used for the photo-catalytic oxidation of cyclohexane is described in detail elsewhere [8]. Briefly, a volume of 50 mL of cyclohexane (99.0% from Sigma Aldrich) was used for the photo-oxidation reactions. Cyclohexane was dried over Molsieve (type 4A) overnight before use, to remove traces of water, and saturated with O_2 by bubbling dry air at 7.65 mL/min. The oxygen-saturated cyclohexane was flown at 4 mL/min through the ATR cell by means of a series II high performance liquid chromatography pump. Prior to the photo-catalytic oxidation experiments, adsorption of cyclohexane on the TiO_2 coating was monitored for 60 min. A spectrum of adsorbed cyclohexane on TiO_2 was collected as background for the photo-oxidation experi-

ment. UV-induced oxidation of cyclohexane was continued for 90 min, taking a spectrum every minute. The photo-catalytic reaction was initiated by an assembly of 7 UV LEDs with 375-nm wavelength emission with an incident photon flux of 9×10^{-9} Einstein $cm^{-2} s^{-1}$ at the surface of the catalyst coating. The first minute of collection was performed in the dark. The background and the sample spectra were averaged from 64 and 32 spectra, respectively. A mirror velocity of $0.6329 cm s^{-1}$ and a resolution of $4 cm^{-1}$ were used for all measurements. All the spectra were corrected by subtracting the features of the rotational modes of water vapor.

2.4. Cyclohexane photo-catalytic oxidation – slurry reactor

Photo-catalytic tests were performed in a slurry reactor illuminated from the top, which will be referred to as top illumination reactor and is described elsewhere [22]. The pyrex reactor contained 100 mL of cyclohexane and 1 g/L of catalyst in all measurements. Air, pre-saturated with cyclohexane was bubbled through the liquid at a flow rate of 30 mL/min, assuring constant saturation of cyclohexane with O_2 (0.012 mol/L). Illumination was provided by a 50-W high pressure mercury lamp (HBO50W from ZEISS), with incident photon flux of 2.10×10^{-7} Einstein $cm^{-2} s^{-1}$ in all measurements. The reaction was carried out for 100 min, and liquid GC samples were analyzed by a flame ionization detector (Chromopack CPwax 52CB).

3. Results

3.1. Characterization

The applied variation of the silylation method yielded a series of materials with different silane loading on TiO_2: TiSi0.1, TiSi1.0, TiSi1.6 and TiSi2.1, which contain 0.1, 1.0, 1.6 and 2.1 wt.% Si, as determined by XRF analysis. Bare Hombikat, of 100% anatase crystallinity, is referred to as TiSi0. The TGA analysis of TiSi0, TiSi1.0, TiSi1.6 and TiSi2.1 recorded in He is shown in Fig. 1. The negative contributions in this figure correspond to the weight loss divided by initial mass of catalyst and are displayed as a function of increasing temperature. At temperatures below 120 °C, weakly adsorbed water is removed from the catalyst surface [15]. More strongly adsorbed water is removed at temperatures between 120 and 300 °C [23], where particle sintering also starts to occur. In the range of 150–400 °C, an extra contribution related to decomposition of HMDS residue may contribute to the weight loss [19]. Above 400 °C, a negative feature is observed for the silylated
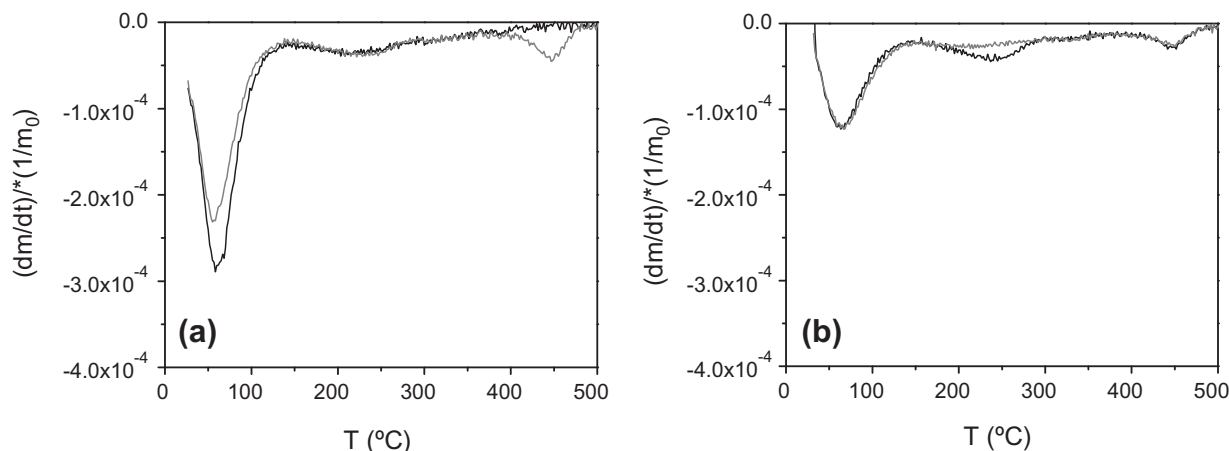

Fig. 1. Thermogravimetric analysis (TGA) under He flow of (a) TiSi0 (black line), TiSi1.0 (gray line) and (b) TiSi1.6 (black line) and TiSi2.1 (gray line).
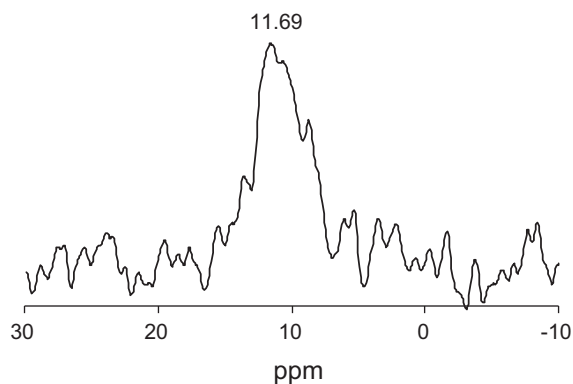
Fig. 2. ^{29}Si MAS NMR of the TiSi1.6 catalyst.

catalysts, which corresponds to the decomposition of methyl groups from the surface silanes [19].

^{29}Si MAS NMR was performed on the TiSi1.6 catalysts to understand which type of Si bonding was induced by the synthesis method. In Fig. 2, a single peak is observed at 11.69 ppm that corresponds to $(TiO)Si(CH_3)_3$ [14,16,19]. Additional NMR features were absent, like those of Si–OH and Si–O–Si groups, so neither

hydroxylation nor polymerization of surface silane groups has occurred to a large extent in the synthesis.

The DRIFTS analysis of the catalysts is shown in Fig. 3a and b. Though different OH active sites have been identified on commercial TiO_2 surfaces, for simplicity, we refer to the surface active sites as acidic or basic OH. The surface OH density was determined by the $Fe(acac)_3$ adsorption method [24], which accounts for all types of OH sites, of which an acidic contribution was measured by NH_3–TPD [7]. The remaining contribution will be referred to as basic OH groups. An acidic/basic OH ratio of 3.3 has been reported for this commercial TiO_2 [7], corresponding to ∼75% surface coverage by acidic OH sites. Stretching vibrations of the acidic OH appear in all spectra, as a number of overlapping bands in the 3690–3630 cm^{-1} region [25] (Fig. 3a). A broad contribution of H_2O is also apparent in the 3600–3000 cm^{-1} region. The basic OH group is H-bridged with adsorbed water molecules, and its stretching vibration is expected to absorb around 3415 cm^{-1} but is overlapped by strong water contributions [25]. The peak area of the acidic OH is represented in Fig. 3c as a function of silane content, and a decreasing trend can be observed. The TiSi0 sample shows small methyl vibrations below 3000 cm^{-1}, characteristic of this commercial TiO_2. A reference spectrum of liquid HMDS is shown in Fig. 3a with specific CH_3 stretching vibrations at 2954 and 2897 cm^{-1}. The silylated materials show similar IR bands but shifted to higher
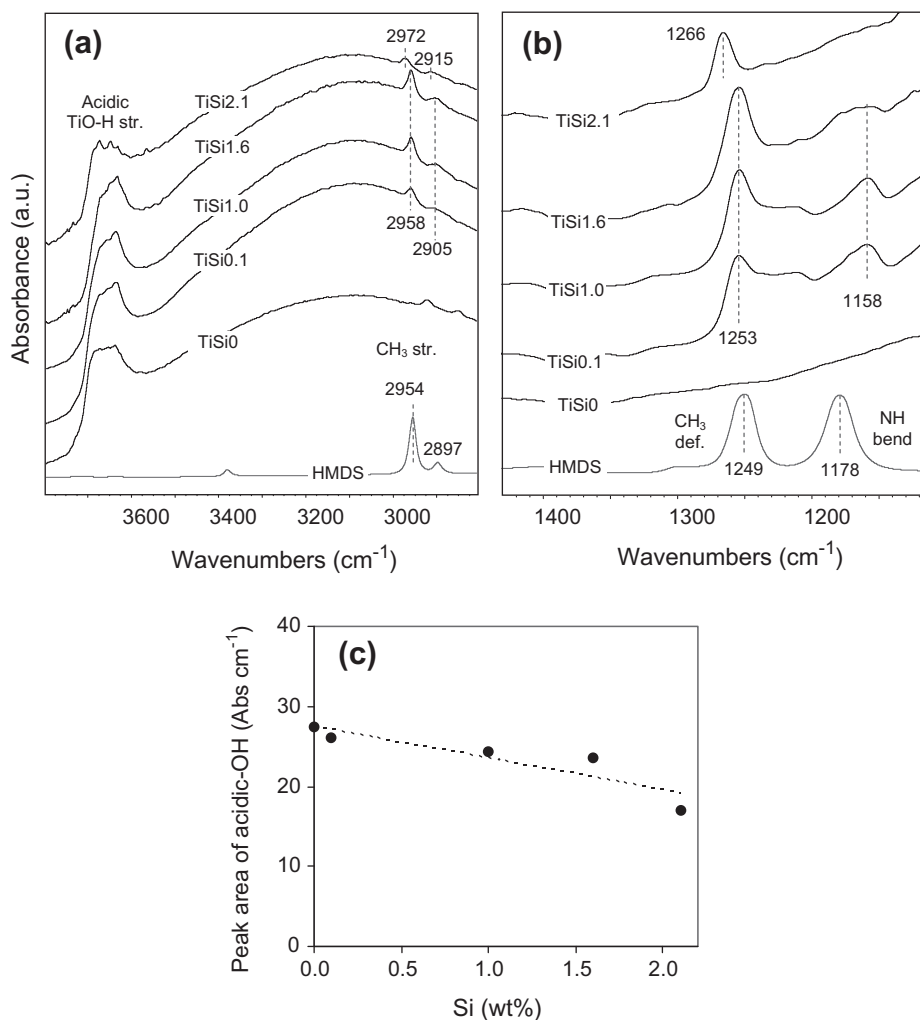

Fig. 3. DRIFTS measurements recorded in He flow of TiSi0, TiSi0.1, TiSi1.0, TiSi1.6 and TiSi2.1 at RT after heating to 120 °C, including a reference spectrum of liquid HMDS, measured by ATR-FTIR in the (a) 3800–2800 cm^{-1} wavenumbers region and (b) the 1450–1100 cm^{-1} wavenumbers region. In (c), the peak area of the acidic TiO–H stretching vibrations is represented as a function of silane content.

wavenumbers, 2958 and 2905 cm^{-1}. The shift is more intense for TiSi2.1, in which the CH$_3$ stretching vibrations of silane occur at 2972 and 2915 cm^{-1}. The typical Si–OH stretching vibration expected at 3675 cm^{-1} [26] is not visible in any of the silylated catalysts, in agreement with the ^{29}Si MAS NMR result.

The spectral features of the samples in the range of 1450–1100 cm^{-1} are shown in Fig. 3b. TiSi0 does not show any particular band in this region, besides the broad feature of strong Ti–O–Ti stretching modes below 1000 cm^{-1}. The silylated TiO$_2$ catalysts show additional IR bands, which are indicative of the presence of surface silane. The reference spectrum of HMDS has specific IR bands at 1249 and 1178 cm^{-1}, which correspond to a CH$_3$ group deformation mode [27] and to NH bending modes [28], respectively. The silylated TiO$_2$ materials show the CH$_3$ group deformation mode [27] at 1253 cm^{-1} and a number of overlapping bands at lower wavenumbers, of which the one occurring at 1158 cm^{-1} is the most pronounced. These bands occur in the NH bending region and are probably related to small amounts of adsorbed NH$_3$ [28,29]. TiSi2.1 shows only the CH$_3$ group deformation mode [27] at 1266 cm^{-1} and no clear NH$_3$ contribution. Other important vibrations like Si–C rocking around 860 cm^{-1} [27], Ti–O–Si stretching vibration at 910–960 cm^{-1} or Si–OH at 980 cm^{-1} [30] are not visible due to the strong absorption modes of TiO$_2$.

3.2. Photo-catalytic cyclohexane oxidation

Fig. 4 shows the ATR-FTIR absorption spectra of the catalysts in cyclohexane flow after 90 min of UV illumination. The acidic OH sites on TiO$_2$ are depleted during the photo-catalytic reaction [8], as witnessed for TiSi0 by the negative vibration centered at 3630 cm^{-1}. The same feature is present in the spectra of the silylated samples, with the higher the silane content, the lower the extent of depletion. The center of the (negative) acidic OH peak shifts from 3630 cm^{-1} on TiSi0 to 3650 cm^{-1} on silylated catalysts, and the relative contribution of this shifted band increases with silane content. In the infrared fingerprint region, below 1800 cm^{-1}, the main products formed during reaction can be observed. The band observed at 1710 cm^{-1} corresponds to the C=O stretching vibration of cyclohexanone, when this molecule is desorbed and dissolved in the reaction mixture. The bands observed at 1691 and 1682 cm^{-1} are also corresponding to the C=O stretching vibration of cyclohexanone but indicate that the molecule is adsorbed on the catalyst surface through hydrogen bonding [8].

The relative absorption of bulk/adsorbed carbonyl bands depends on the degree of silylation. In TiSi0, the bulk cyclohexanone band intensity is much lower than the bands corresponding to adsorbed cyclohexanone. Silylated samples show a similar bulk cyclohexanone band as observed for TiSi0, but lower contributions of adsorbed cyclohexanone. The formation of other species is also apparent in the region below 1600 cm^{-1}, where a broad absorption of at least three main bands is apparent. Different species can contribute to these absorptions, including symmetric vibrations of carboxylates [31,32], carbonates (around 1589 cm^{-1}) [33] and bicarbonates (around 1555 cm^{-1}) [34]. These species adsorb strongly on the TiO$_2$ surface and are therefore referred to as deactivating species. The CH$_3$ bending vibration of the silane groups shows a negative absorption after the photo-catalytic reaction. The position of these negative bands is at 1247 cm^{-1} for samples of low silane content and at 1256 cm^{-1} for TiSi2.1. These bands are slightly red shifted in comparison with the ones observed in Fig. 3.

The peak heights of the 1691, 1579 and 3630 cm^{-1} bands after 90 min of photo-catalytic reaction were determined for all catalysts and are shown in Fig. 5, as a function of silane content. The
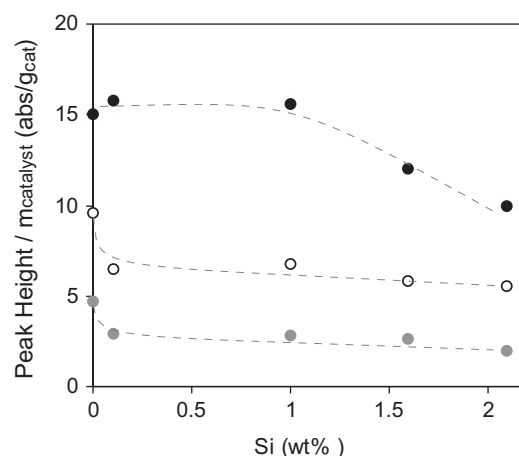
Fig. 5. ATR-FTIR bands after 90 min of cyclohexane photo-oxidation for TiSi0, 0.1, 1.0, 1.6 and 2.1 divided by the mass of catalyst. The black symbols correspond to deactivating species (1579 cm^{-1}), the empty symbols to adsorbed cyclohexanone (1691 cm^{-1}) and the gray symbols to the positive values of acidic OH depletion (3630 cm^{-1}).
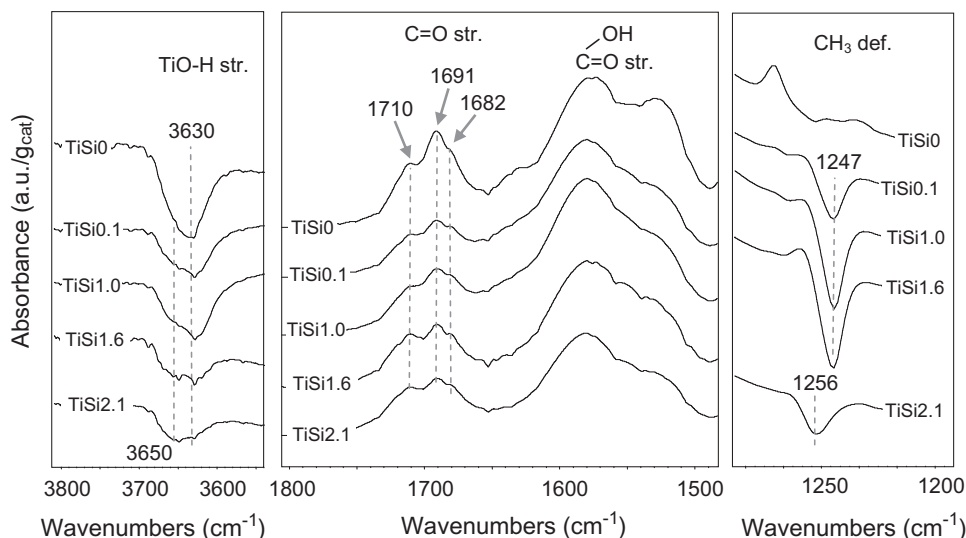
Fig. 4. ATR-FTIR spectrum after 90 min of cyclohexane photo-oxidation on TiSi0, TiSi0.1, TiSi1.0, TiSi1.6 and TiSi2.1.

band height for adsorbed cyclohexanone decreases with silane content. The peak height of the acidic OH depletion is represented by positive values, showing a decrease with surface silane concentration. Both adsorbed cyclohexanone and acidic OH depletion show a similar trend. From the intensity of the band of deactivating species represented by the absorption at 1579 cm^{-1}, it can be concluded that the amount of deactivating species formed decreases only above 1.0% silane content.

### 3.3. Cyclohexanone and water desorption under dark conditions

Cyclohexanone and water desorption were analyzed after reaction in the ATR-FTIR setup, by continuing the cyclohexane flow under dark conditions. Cyclohexanone desorption is characterized by a decay in the intensity of the 1691 cm^{-1} band in time, which is shown in Fig. 6a, for the TiSi0, TiSi1.0 and TiSi2.1 catalysts. Although carboxylates and water might have a small contribution to the peak height of the 1691 cm^{-1} band, exponential curves could be well fitted through the data, allowing estimation of the desorption constants of cyclohexanone through the following equation: $H = H_0 \exp(k_{des}t) + H_{end}$, where k_{des} is the desorption constant of cyclohexanone, measured in 1/min, while H is the 1691 cm^{-1} peak height in time, H_0 the peak height at $t = 0$ min and H_{end} the peak height at $t = 60$ min, all determined in absorbance/$g_{catalyst}$. TiSi0 starts from a larger value of H_0 but for all cases a similar H_{end} is reached after 60 min of dark desorption. The k_{des} values deduced from the exponential decay in all catalysts are represented in Fig. 6b as a function of silane content, and a linear relation was obtained.

A similar result was obtained for water desorption after reaction, shown in Fig. 7a. The amount of water desorbing from TiSi0 is much larger than for silylated materials, indicating a higher degree of surface hydration. The exponential curves fitted through the data provide an estimate for the desorption constant of water from the surface, which is represented in Fig. 7b as a function of silane content. As for cyclohexanone, it can be observed that k_{des} for water correlates linearly with surface silylation.
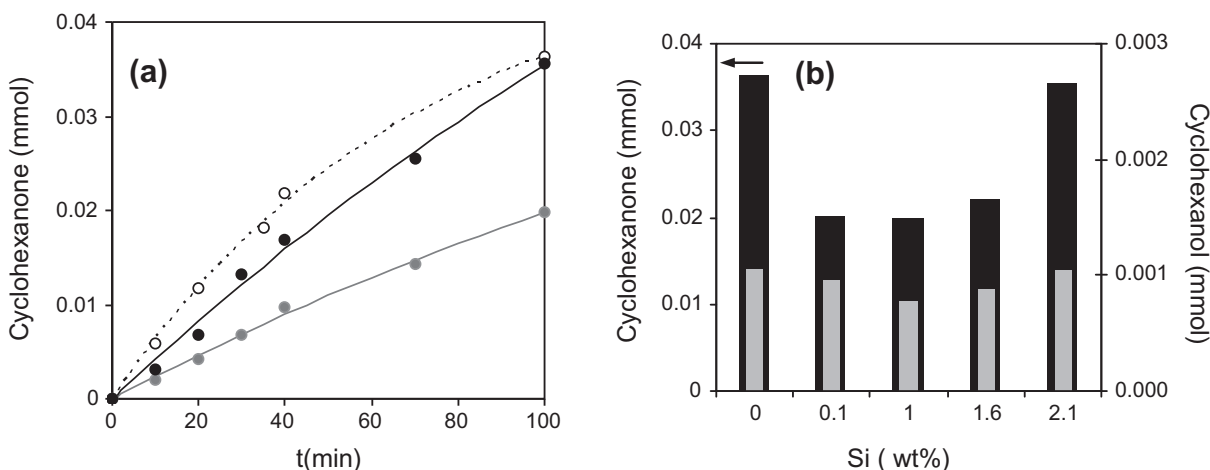
3.4. Top illumination reactor

To compare the performance of the different catalysts in a quantitative way, cyclohexane photo-oxidation tests were
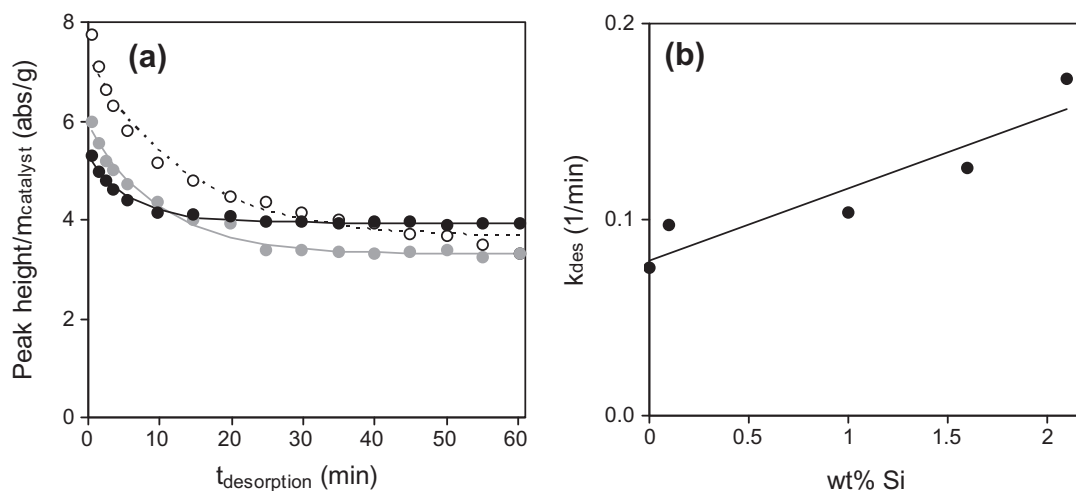
Fig. 6. (a) Cyclohexanone desorption (dark conditions) on TiSi0 (open symbols), TiSi1.0 (gray symbols) and TiSi2.1 (black symbols) measured by the 1691 cm^{-1} band height divided by catalyst mass (the lines correspond to exponential fits) and (b) cyclohexanone desorption constant (determined from the exponential curves) as a function of silane content (wt.%).
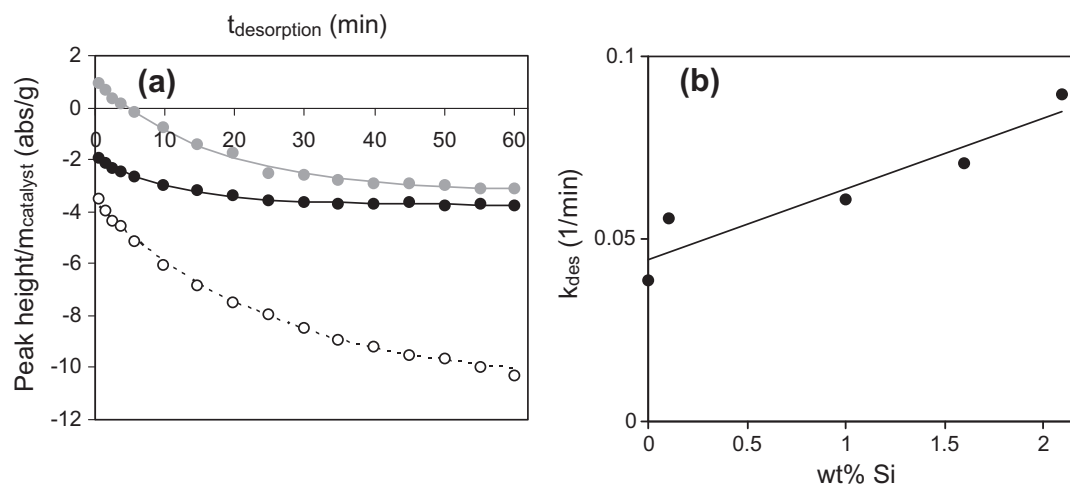
Fig. 7. (a) Water desorption (dark conditions) from TiSi0 (open symbols), TiSi1.0 (gray symbols) and TiSi2.1 (black symbols) measured by the 3350 cm^{-1} band height divided by catalyst mass (the lines correspond to exponential fits) and (b) water desorption constant (determined from the exponential curves) as a function of silane content (wt.%).

Fig. 8. GC analysis of the products of cyclohexane photo-oxidation performed in a top illumination reactor. (a) Formation of cyclohexanone (in mmol) in time for TiSi0 (open symbols), TiSi1.0 (gray symbols) and TiSi2.1 (black symbols) and (b) cyclohexanone (black) and cyclohexanol (gray) in mmol, formed after 100 min of reaction, for all catalysts.

performed in a top illumination reactor. Fig. 8a shows the photo-catalytic formation of cyclohexanone in mmol, for TiSi0, TiSi1.0 and TiSi2.1. The initial rate of cyclohexanone formation increases in the following order: TiSi0 > TiSi2.1 > TiSi1.0. At illumination times longer than 40 min, the slope of the TiSi0 and TiSi1.0 curves decreases due to deactivation, and the rate of cyclohexanone formation for TiSi2.1 becomes the highest. Fig. 8b shows the GC results after 100 min of reaction for all the catalysts, for both cyclohexanone and cyclohexanol (in mmol). The latter was not clearly observed in the ATR-FTIR results, but in the slurry reactor cyclohexanol is observed, though in very low amounts for all samples. Cyclohexanone formation decreases by addition of small amounts of silane to the TiO$_2$ surface, but over 1.0 wt.% Si the amount of cyclohexanone formed increases again. For TiSi2.1, the ketone formed after 100 min of photo-oxidation is similar to that obtained for bare TiO$_2$. The selectivity toward cyclohexanone formation is similar, ranging between 95% and 97%, suggesting that the reaction mechanism is not affected by silylation.

4. Discussion

HMDS is expected to react with a TiO$_2$ surface through the equation described in Fig. 9 [18].

We provide significant evidence that indeed this reaction has occurred on the Hombikat surface. The XRF analysis proves the presence of silicon on the TiO$_2$ surface, with a range of 0 up to 2.1 wt.% Si loading, corresponding to a maximum surface coverage of 60%. Silane coupling on the surface is furthermore demonstrated

by the ^{29}Si MAS NMR (Fig. 2) spectra, in which isolated Ti–O–Si(CH$_3$)$_3$ groups were identified for TiSi1.6. Since not all catalysts were analyzed by ^{29}Si MAS NMR, other types of silane coupling for samples containing higher silane content cannot be excluded. Silylation is confirmed by DRIFTS analysis (Fig. 3), where the presence of methyl groups with wavenumbers corresponding to those of HMDS on the surface is evident. Also secondary changes in the surface properties are in agreement with surface silylation. TGA analysis in Fig. 1 shows a lower amount of weakly and strongly adsorbed water on the surface, indicating that TiO$_2$ catalysts become less hydrophilic after the silylation procedure. This is confirmed by the decreasing intensity of absorptions assigned to water vibrations in the DRIFT spectra (Fig. 3). Furthermore, from the DRIFT spectra, it can be deduced that acidic OH groups are converted, the amount changing linearly with silane content (Fig. 3c). The analysis of basic OH sites is not possible under the applied conditions, so the possibility of silylation of basic OH sites cannot be fully ruled out. But knowing that (i) only ~25% of the OH sites existing on the surface are basic [7], (ii) the maximum coverage with silylated species is 60% (for TiSi2.1) and (iii) a linear relation with the amount of acidic sites exists, we conclude that mainly acidic sites are silylated. It is therefore proposed that silanes bind to the TiO$_2$ surface preferentially through the acidic OH sites, as demonstrated in Fig. 9. It can be concluded that for TiSi2.1 the acidic OH is not fully depleted upon silylation. This is important because both acidic and basic OH sites are involved in cyclohexane photo-oxidation, as proposed in a previously reported reaction mechanism [8]. Another factor preventing full silylation is the coverage of the TiO$_2$ surface with up to three hydrogen-bonded water
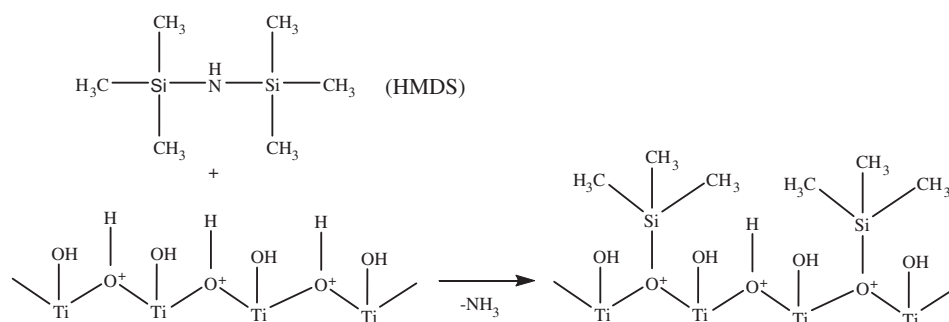
Fig. 9. Expected reaction of Hexamethyldisilazane (HMDS) with TiO$_2$, producing a partially silylated TiO$_2$ surface and ammonia.

layers at ambient conditions, of which some is strongly adsorbed [23,35]. A pre-treatment at temperatures higher than 400 °C, needed for complete dehydration (Fig. 1), was not applied in this study, in order to prevent morphological changes and to maintain a comparable activity of the samples. Summarizing, the synthesis procedure leads to a successful partial silylation of the TiO2 surface.

4.1. Cyclohexanone and water desorption

The main objective of this study was to decrease the surface hydrophilicity of TiO2, by coupling hydrophobic groups on the surface and stimulate desorption of photo-catalytically formed cyclohexanone. The polar character of cyclohexanone and water molecules leads to desorption times from TiO2 into an organic medium of over 30 min [9]. As desired, the cyclohexanone and water desorption constants were significantly increased by silylation (Figs. 6 and 7). Since the desorption constants of both cyclohexanone and water increase linearly with surface silane content, we propose that the adsorption enthalpy of these molecules on surface OH sites decreases by the presence of neighboring silane groups. A progressive shift of the negative band from 3630 to 3650 cm^{-1} with increasing silane content (Fig. 4), suggesting a decrease in acid strength of the OH groups, is in agreement with weaker product adsorption involving H bridges.

The increased rate of desorption indicated earlier leads to a lower amount of deactivating species on the surface of catalysts with more than 1.0 wt.% Si (Figs. 4 and 5). This can be explained as follows. It has been previously proposed that the main route for carboxylate formation is through the oxidation of surface-bound cyclohexanone by ·OH radicals [8]. The increased hydrophobicity of the surface decreases the amount of adsorbed water, thus decreasing the concentration of ·OH radicals formed during illumination. The smaller availability of ·OH radicals contributes to the observed larger surface selectivity.

Though the cyclohexanone desorption rates are increased and, as a consequence, catalyst deactivation is reduced, surface silanes proved to be unstable under photo-catalytic conditions (Fig. 4). The negative trend in the CH3 deformation vibration indicates that the silane groups are oxidized, as observed in previous publications [17]. Analyzing the catalyst coating before and after reaction (not shown), we observed that the decomposition of the silanes from the surface is not complete, explaining the observed remaining positive effects. No evidence was found for the recovery of OH sites

characteristic of the (silane-free) TiSi0 sample, upon UV illumination of silylated catalysts. Perhaps the best strategy is to apply more stable silane groups, e.g., fluorine-containing silylation agents, that have been confirmed to be very stable under photo-catalytic conditions [36].

4.2. Effect of silylation on the reaction rate

In silylating the catalyst surface, the number of available active OH sites is reduced, so an effect on the rate of cyclohexanone formation is expected [22]. In Fig. 10a, the initial rate of cyclohexanone formation is compared to the rate over partially deactivated catalysts, as determined from the tangents of the exponential fits at $t = 0$ min and $t = 100$ min in Fig. 8a. The initial reaction rate is greatly decreased for catalysts with low silane content, but at silane loadings above 1.0% there is an increase in the initial rate of cyclohexanone formation. The large difference in initial rate observed for TiSi0 relative to the silylated samples suggests the presence of a fraction of highly reactive sites on the surface. These highly reactive sites are apparently preferentially converted to Ti–O–Si(CH3)3 groups upon silylation or blocked by NH3 adsorption during silylation (Fig. 3). We conclude that these highly active sites are very susceptible to deactivation, explaining the large difference between initial cyclohexanone formation rate and the rate over partially deactivated TiSi0 catalyst, compared to the silylated materials. In the following, we provide a simplified explanation to the trend in cyclohexanone formation rate over partially deactivated surfaces, on the basis of the trend in desorption rate constant, and availability of acidic OH sites, taken as a measure of the photo-catalytic sites (Fig. 10b).

The rate of cyclohexanone formation, r in mmol/min, can be described by Eq. (1):

$$r = k_f N_T \frac{K_{Cane} C_{Cane}}{1 + K_{Cane} C_{Cane} + K_{Cnone} C_{Cnone}} \tag{1}$$

where k_f (min/mmol) is the cyclohexanone formation constant, N_T the number of available active sites (OH groups, lowered in amount by catalyst deactivation and precursors for the active site formed by light activation), K_{Cane}, C_{Cane} (mmol/cm^3) and K_{Cnone}, C_{Cnone} (mmol/cm^3) the Langmuir constants and concentrations of cyclohexane and cyclohexanone, respectively. Because of the low temperatures, it is assumed that the occupancy is high, implying that the fraction of empty sites is negligible. Two limiting cases are considered.
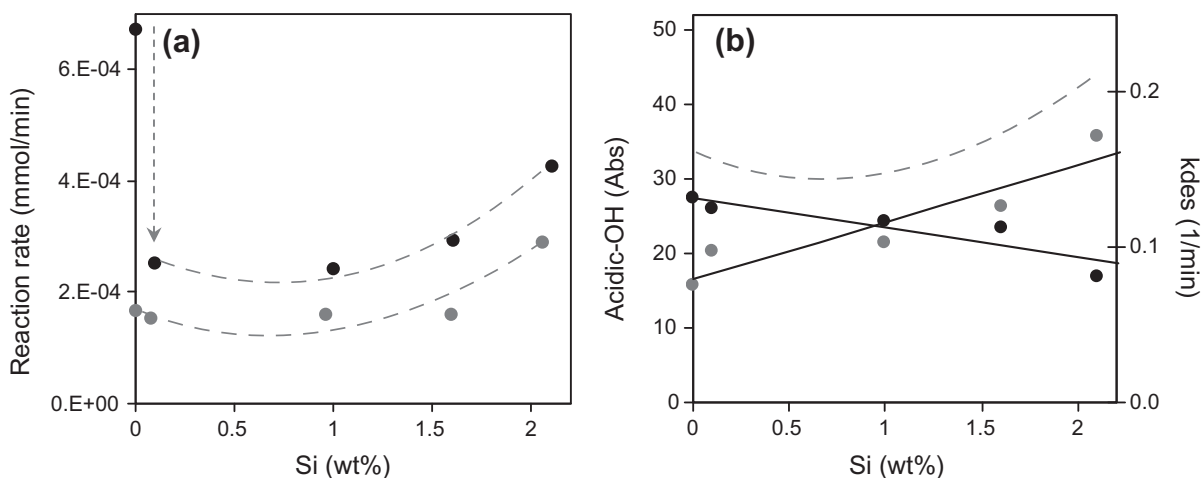
Fig. 10. (a) Initial cyclohexanone formation rate (black symbols) and rate over partially deactivated surfaces (gray symbols) during photo-catalytic cyclohexane oxidation, as determined in the top illumination reactor. The arrow emphasizes the large difference in initial cyclohexanone formation rate between TiSi0 and TiSi0.1. (b) Peak area of acidic OH (black) and cyclohexanone desorption constant (gray) as a function of silane content, compared with the cyclohexanone formation rate over partially deactivated surfaces (dashed gray line).

When $K_{Cane}C_{Cane} \gg [1 + K_{Cnone}C_{Cnone}]$, Eq. (1) can be simplified to:

$$r = k_f N_T \tag{2}$$

When $K_{Cnone}C_{Cnone} \gg [1 + K_{Cane}C_{Cane}]$, Eq. (1) can be simplified to:

$$r = k_f N_T \frac{K_{Cane}C_{Cane}}{K_{Cnone}C_{Cnone}} \tag{3}$$

Cyclohexanone is expected to have a much stronger adsorption enthalpy than cyclohexane, so the second limiting case is most realistic and considered in the following. For simplicity, we assume that on bare TiO_2 only one set of OH sites determines the reaction rate in steady-state conditions ($N_{T,TiSi0} = N_1$). On a silylated surface, three types of sites are distinguished: isolated OH sites (N_1), OH sites with a neighboring silane group (N_2) and silylated inactive sites (N_{Si}), $N_T = N_1 + N_2 + N_{Si}$. So for a silylated surface $[N_1 + N_2] < N_{T,TiSi0}$.

This leads to the following rate equation:

$$r = k_f N_1 \frac{K_{Cane}C_{Cane}}{K_{Cnone,1}C_{Cnone}} + k_f N_2 \frac{K_{Cane}C_{Cane}}{K_{Cnone,2}C_{Cnone}} \tag{4}$$

For TiSi0 this reduces to:

$$r_{TiSi0} = k_f N_{T,TiSi0} \frac{K_{Cane}C_{Cane}}{K_{Cnone,1}C_{Cnone}} \tag{5}$$

The trends in surface OH sites ($N_1 + N_2$), assuming that the acidic OH groups represent the active sites, and desorption constants (k_{des}) as a function of silylation are shown in Fig. 10b.

The data shows for TiSi2.1: ($N_1 + N_2$) = $0.6N_{T,TiSi0}$. It should be noted that for TiSi2.1, a surface coverage of 60% was obtained and, as a consequence, the number of OH active sites which are neighboring a silane group is predominant, so $N_2 \gg N_1$ and $N_2 \sim 0.6N_{T,TiSi0}$. For the rate of desorption of TiSi2.1, an analogous relation holds: $k_{des,TiSi2.1} = 2.3\ k_{des,TiSi0}$, which corresponds to $K_{Cnone,TiSi2.1} = (1/2.3)K_{Cnone,TiSi0}$ (when k_{ads} is constant). So Eq. (4) for TiSi2.1 can be simplified to:

$$r_{TiSi2.1} = k_f 0.6 N_{T,TiSi0} \frac{K_{Cane}C_{Cane}}{(1/2.3)K_{Cnone,1}C_{Cnone}} = 1.4 r_{TiSi0} \tag{6}$$

assuming that the cyclohexanone formation rate constant is the same for TiSi0 and TiSi2.1. So the rate of cyclohexanone formation is higher for TiSi2.1 than for TiSi0 due to the improved desorption constant, despite the decrease in available active sites. Accordingly, the available OH sites of TiSi2.1, taking into consideration that approximately 60% of the OH groups is converted by silylation, show a higher turnover frequency than of TiSi0, i.e., $9.3 \times 10^{-3}\ min^{-1}$ compared to $5.6 \times 10^{-3}\ min^{-1}$, respectively. The turnover numbers are 0.8 and 0.3 for TiSi2.1 and TiSi0 for the short illumination time applied here. Previous work has shown that TiSi0 at longer illumination times shows a TON above unity and that (silylated) TiO_2 is indeed a catalyst for the target reaction, albeit deactivating.

As stated previously, Eq. (6) applies only to the rate of cyclohexanone formation at prolonged illumination times, after which a certain amount of active sites is deactivated. To analyze the initial rate of cyclohexanone formation on TiSi0, two sites should be considered: very reactive, rapidly deactivating OH sites (N_3) and the stable OH sites contributing to the conversion over partially deactivated catalysts (N_1). The cyclohexanone formation constant for N_3 (k_3) is apparently considerably larger than for N_1 (k_1). This has an effect on the photonic efficiency, determined by the ratio of the initial rate of product formation and the incident photon flux, which is higher for TiSi0 (0.0025 in mol Einstein^{-1}) than for TiSi2.1 (0.0016 in mol Einstein^{-1}). It should be mentioned that in the final stages of the reaction, the photonic efficiency is higher for TiSi2.1

(0.00108 in mol Einstein^{-1}) than for TiSi0 (0.00062 in mol Einstein^{-1}), the consequence of the much slower rate of deactivation of the silylated catalyst.

In summary, the data show that a relatively high level of silylation is required to create improved catalysts. Two regimes can be defined:

(1) At Si content <1.0 wt.%, the rate of cyclohexanone formation follows the decrease in available OH sites. So the improvement in cyclohexanone desorption rate constant is not enough to compensate for the decrease in surface OH groups.
(2) At Si content >1.0 wt.%, the rate of cyclohexanone formation increases as a result of a further increased cyclohexanone desorption rate constant. Under these conditions, the desorption rate becomes dominant and over-compensates the negative impact of the decrease in surface OH groups. At higher silane content, the still available OH sites are characterized by a higher turnover frequency than the original free OH sites on TiSi0.

There should be an optimum silane loading that combines the increased surface hydrophobicity, with a sufficient number of available surface active sites. Based on the data provided here, the silylation loading should be at least 2.1 wt.%.

5. Conclusions

A commercial TiO_2 catalyst was modified by coupling $-Si(CH_3)_3$ groups to its surface. The silane groups, which seems to react preferentially with acidic OH sites, increase the hydrophobicity of the silylated-TiO_2 catalysts. Desorption rates of cyclohexanone were increased by surface modification, and a linear relation between silane loading and cyclohexanone desorption rate constant was observed. Accordingly, during cyclohexane photo-oxidation, the silylated catalysts showed lower tendency for deactivation. At low silane contents, the rate of cyclohexanone formation over partially deactivated surfaces decreased due to the dependency on the number of OH groups. However, for higher silane content (Si > 1.0 wt.%), the increased desorption rate of cyclohexanone overcomes the lower number of surface OH sites with relatively high stability.

The silylated surface groups were not stable under photo-catalytic conditions. Improvement of the surface modification method should include the use of fluorine-containing silylation agents, which have been proven to resist photo-catalytic conditions.

References

[1] A. Fujishima, X.T. Zhang, C.R. Chim 9 (2006) 750.
[2] A. Mills, R.H. Davies, D. Worsley, Chem. Soc. Rev. 22 (1993) 417.
[3] M.A. Fox, M.T. Dulay, Chem. Rev. 93 (1993) 341.
[4] J. Peral, X. Domenech, D.F. Ollis, J. Chem. Technol. Biotechnol. 70 (1997) 117.
[5] H. Einaga, S. Futamura, T. Ibusuki, Appl. Catal. B – Environ. 38 (2002) 215.
[6] S.A. Larson, J.L. Falconer, Catal. Lett. 44 (1997) 57.
[7] P. Du, J.A. Moulijn, G. Mul, J. Catal. 238 (2006) 342.
[8] A.R. Almeida, J.A. Moulijn, G. Mul, J. Phys. Chem. C 112 (2008) 1552.
[9] T.J.A. Renckens, A.R. Almeida, M.R. Damen, M.T. Kreutzer, G. Mul, Catal. Today, in press, doi:10.1016/j.cattod.2009.12.002.
[10] C.B. Almquist, P. Biswas, Appl. Catal. A – Gen. 214 (2001) 259.

[11] M.A. Brusa, Y. Di Iorio, M.S. Churio, M.A. Grela, J. Mol. Catal. A – Chem. 268 (2007) 29.
[12] P. Boarini, V. Carassiti, A. Maldotti, R. Amadelli, Langmuir 14 (1998) 2080.
[13] W. Mu, J.M. Herrmann, P. Pichat, Catal. Lett. 3 (1989) 73.
[14] N. Igarashi, K. Hashimoto, T. Tatsumi, Micropor. Mesopor. Mater. 104 (2007) 269.
[15] M.V. Cagnoli, S.G. Casuscelli, A.M. Alvarez, J.F. Bengoa, N.G. Gallegos, M.E. Crivello, E.R. Herrero, S.G. Marchetti, Catal. Today 107–08 (2005) 397.
[16] M.L. Pena, V. Dellarocca, F. Rey, A. Corma, S. Coluccia, L. Marchese, Micropor. Mesopor. Mater. 44 (2001) 345.
[17] S. Ikeda, Y. Kowata, K. Ikeue, M. Matsumura, B. Ohtani, Appl. Catal. A – Gen. 265 (2004) 69.
[18] M.I. Baraton, L. Merhari, J. Eur. Ceram. Soc. 24 (2004) 1399.
[19] X.F. Li, H.X. Gao, G.J. Jin, L. Chen, L. Ding, H.Y. Yang, Q.L. Chen, J. Mol. Struct. 872 (2008) 10.
[20] A. Quintanilla, J.J.W. Bakker, M.T. Kreutzer, J.A. Moulijn, F. Kapteijn, J. Catal. 257 (2008) 55.
[21] A.Y. Fadeev, R. Helmy, S. Marcinko, Langmuir 18 (2002) 7521.
[22] J.T. Carneiro, C.C. Yang, J.A. Moma, J.A. Moulijn, G. Mul, Catal. Lett. 129 (2009) 12.
[23] J. Soria, J. Sanz, I. Sobrados, J.M. Coronado, A.J. Maira, M.D. Hernandez-Alonso, F. Fresno, J. Phys. Chem. C 111 (2007) 10590.
[24] J.A. Rob van Veen, Fred T.G. Veltmaat, Gert Jonkers, J. Chem. Soc. Chem. Commun. (1985) 1656.
[25] G. Martra, Appl. Catal. A – Gen. 200 (2000) 275.
[26] T.A. Jurgens, J.W. Rogers, J. Phys. Chem. 99 (1995) 731.
[27] L.J. Bellamy (Ed.), The Infrared Spectra of Complex Molecules Advances in Infrared Group Frequencies, Chapman and Hall Ltd., London, 1975.
[28] G. Busca, H. Saussey, O. Saur, J.C. Lavalley, V. Lorenzelli, Appl. Catal. 14 (1985) 245.
[29] K. Hadjiivanov, O. Saur, J. Lamotte, J.C. Lavalley, Z. Phys. Chem. – Int. J. Res. Phys. Chem. Chem. Phys. 187 (1994) 281.
[30] C. Beck, T. Mallat, T. Burgi, A. Baiker, J. Catal. 204 (2001) 428.
[31] P.Z. Araujo, C.B. Mendive, L.A.G. Rodenas, P.J. Morando, A.E. Regazzoni, M.A. Blesa, D. Bahnemann, Colloid Surf. A – Physicochem. Eng. Aspects 265 (2005) 73.
[32] D.J. Yates, J. Phys. Chem. 65 (1961) 746.
[33] W.G. Su, J. Zhang, Z.C. Feng, T. Chen, P.L. Ying, C. Li, J. Phys. Chem. C 112 (2008) 7710.
[34] M. Primet, P. Pichat, M.V. Mathieu, J. Phys. Chem. 75 (1971) 1221.
[35] A.Y. Nosaka, Y. Nosaka, Bull. Chem. Soc. Jpn. 78 (2005) 1595.
[36] Y. Kuwahara, K. Maki, Y. Matsumura, T. Kamegawa, K. Mori, H. Yamashita, J. Phys. Chem. C 113 (2009) 1552.